ORIGINAL PAPER

D. J. Cooke · S. E. Redfern · S. C. Parker

Atomistic simulation of the structure and segregation to the (0001) and (01$\bar{1}$2) surfaces of Fe$_2$O$_3$

Abstract The segregation of ten isovalent impurities (Al^{3+} Cr^{3+}, Eu^{3+}, Gd^{3+}, Ho^{3+}, La^{3+}, Lu^{3+}, Nd^{3+}, Tb^{3+}, Y^{3+}) to the (01$\bar{1}$2) and the (0001) surfaces of haematite (α-Fe$_2$O$_3$) have been studied using atomistic simulation where the forces between the atoms are modelled using the Born model of solids. Segregation is found to be energetically favoured in virtually every case. The results for the (01$\bar{1}$2) surface show that the most favourable impurity surface concentration is 33.33%. The (0001) surface has two possible terminations, one terminated by iron atoms and the other by oxygen. No minimum is calculated for the Fe termination of the (0001) surface at low temperatures, but when the effect of raising the temperature is considered, an energy minimum is found, also at 33.33% impurity coverage. In contrast, the O terminated (0001) surface has a minimum in the segregation energy for between 16.67 and 33.33% depending on the cation being considered.

Keywords Surface of haematite · Low index surfaces · Segregation · Atomistic simulation

Introduction

The aim of the work described in this paper is to investigate the segregation of a number of isovalent heavy metal impurities from the bulk structure to two of the most stable low index surfaces of haematite (α-Fe$_2$O$_3$).

Impurities are known to segregate to the interfaces of many solids (Mackrodt et al. 1985; Cotter et al. 1989; Davies et al. 1989; Janowski et al. 1991; Harding et al. 2003) and if there is significant segregation, the composition and hence the behaviour of the surfaces will change. Such differences in composition can be observed when materials with impurities are heated, as this causes the impurities to be concentrated at the surfaces (Suzuki et al. 1998). The resulting change in the surface composition will affect a range of properties from the sintering, adsorption and reactivity of the mineral. Thus, understanding the extent to which impurities segregate to specific surfaces is a necessary first step towards predicting the effect of impurities on surface properties.

Since iron oxide surfaces are amongst the most reactive species found in soils (Arocena et al. 1992), there is a need for studying the interaction with impurities. These include the interaction with chromium ions (Kendelewicz et al. 1999) and radionuclides (Wenming 2001). The latter is of interest for determining a mechanism for immobiliing radionuclides from both disposal sites and reactor accident zones. Clearly in soil processes solvent and organic matter are important (Bryan et al. 1998; Xiangke et al. 2000); however, in order to understand the segregation of such heavy metals from the bulk structure to the most stable surfaces of a significant soil mineral (α–Fe$_2$O$_3$), it is necessary to separate out the different factors controlling surface structure and stability. One method that can achieve this is atomistic simulation. A second motivation for this work is that if atomistic simulation can be used to calculate the optimum composition of a given surface, then the approach could provide possible suggestions for further experimental investigation, especially if the surface composition represents a technologically useful material.

The segregation of impurities to pure/dry surfaces therefore represents a clear starting point for such an investigation. In addition, it also provides data for comparison with experiments on surfaces examined under ultra-high vacuum conditions. Before discussing these results, the methodology adopted and a brief discussion of the structure of haematite, its low index surfaces and their relative stability is included. This focuses on the two significant surfaces of haematite, namely the (01$\bar{1}$2) and (0001) surfaces.

D. J. Cooke · S. E. Redfern · S. C. Parker (✉)
Department of Chemistry, University of Bath,
Bath, BA2 7AY UK
e-mail: s.c.parker@bath.ac.uk

Theory and methodology

The work described in this paper was carried out using atomistic simulation techniques based on the Born model of solids (Born and Haung 1954). The long-ranged Coulombic interactions are calculated using Parry's modification of the Ewald summation (Ewald 1921 Parry 1975, 1976). The short-range interactions such as repulsions between adjacent atoms and van der Waals forces are represented by simple, parameterized, analytical functions such as the Buckingham potential, which takes the form:

$$\Phi_{ij}(r_{ij}) = A_{ij}\exp(-r_{ij}/\rho_{ij}) - C_{ij}/r_{ij}^6,$$

where A_{ij}, ρ_{ij} and C_{ij} are parameters particular to each pair-wise interaction and r_{ij} is the separation between atom i and atom j.

The potential model parameters used for haematite and the isovalent impurities are based on those derived by Lewis and Catlow (1985), see Table 1. In all cases the oxide ion is described using the Dick and Overhauser (1958) shell model to simulate the polarizability. In this approach the anions are represented by a core and massless shell, which are connected by a spring. The charges of the core and shell along with the spring constant determine the polarizability of the ion. We consider the cations to be unpolarizable.

The structures and surface energies were calculated using the METADISE code (Watson et al. 1996), which follows the approach of Tasker (1979), whereby the crystal is divided into two blocks, each comprising a region I and a region II. Region I contains the ions closest to the surface and region II is composed of more distant ions. In the simulation, the ions in region I can relax whilst the region-II ions are held fixed at their bulk positions. The sizes of region I and region II must be large enough to ensure that the energy is converged. In this study we found that a region I of depth 15 Å and a region II of depth 150 Å was sufficient. A short range cutoff of 15 Å was used.

Table 1 Buckingham potentials used to describe the isovalent cations used in the segregation studies. (Lewis and Catlow 1985)

		A (eV)	P (Å)	C (eV Å^{-6})
Al core	O shell	1114.9	0.3118	0.0
Cr core	O shell	1734.1	0.3010	0.0
Eu core	O shell	1358.0	0.3556	0.0
Gd core	O shell	1336.8	0.3551	0.0
Ho core	O shell	1350.2	0.3487	0.0
La core	O shell	1439.7	0.3651	0.0
Lu core	O shell	1347.1	0.3430	0.0
Nd core	O shell	1379.9	0.3601	0.0
Tb core	O shell	1369.7	0.3521	0.0
Y core	O shell	1345.1	0.3491	0.0
Fe core	O shell	1102.4	0.3299	0.0
O shell	O shell	22764.0	0.1490	27.88

	Mass/au	Charge/au
Fe core	55.847	3.00
O core	15.9994	0.21
O shell	0.00	−2.21
Al core	26.92	3.00
Cr core	52.00	3.00
Eu core	151.96	3.00
Gd core	157.25	3.00
Ho core	164.93	3.00
La core	138.91	3.00
Lu core	174.97	3.00
Nd core	144.24	3.00
Tb core	158.93	3.00
Y core	88.91	3.00

	k/eV Å^{-2}	
O shell – O core	27.4	

The surface energy (γ) is defined as the surface excess energy per unit area of a block of crystal containing the surface, E_{surf}, relative to a block containing an equivalent number of ions in the bulk, E_{bulk}. It is defined as:

$$\gamma = \frac{(E_{surf} - E_{bulk})}{\text{Area}} .$$

A small positive value of γ represents a stable surface.

Ten iso-valent cations, namely Al^{3+} Cr^{3+}, Eu^{3+}, Gd^{3+}, Ho^{3+}, La^{3+}, Lu^{3+}, Nd^{3+}, Tb^{3+}, Y^{3+}, were chosen for study and each was substituted into each surface, replacing a varying number of surface Fe^{3+} ions.

As a way of exploring a number (but not an excessive number) of configurations, the orientated cells were scaled so that there were six surface cations, enabling different concentrations of impurity to be considered. All the resulting configurations were then energyminimized. Many non-equivalent configurations were considered and the lowest energy configurations are reported. The segregation energy per dopant cation is defined as the energy difference between placing an impurity in the surface with that of placing the same impurity in the bulk and is given by:

$$E_{seg} = ((E_{surf+defect} - E_{surf})/n) - (E_{bulk} + \text{defect} - E_{bulk}) ,$$

where E_{surf}, as noted above, is the energy of the pure surface, n is the number of impurity ions on the surface. $E_{surf+defect}$ is the energy of the surface containing n impurity ions and ($E_{bulk+defect} - E_{bulk}$) is the energy of an isolated impurity ion in the bulk structure, which was calculated along with the energy associated with creating an isolated surface defect using the well-known Mott and Littleton (1938) approach implemented in the programs CASCADE (Leslie 1982) (for bulk defects) and CHAOS (Duffy and Tasker 1983) (for surface defects).

It is, however, possible to go beyond the calculation of the static lattice energy of a system and calculate the vibrational contribution to the free energy using lattice dynamics Parker (2001). We follow the work of, for example Born and Huang (1954), Cochran (1973) and Barron et al. (1980) which is implemented in the code: PARAPOCS (phonon-assisted relaxation applied to the prediction of crystal structures) (Parker and Price 1989; Watson et al. 1994). The approximation here is to use the theory of small amplitude vibrations. The lattice potential energy is expanded as a power series of the displacement of the atoms from their minimum energy positions, but only to the second order. The equations of motion are then linear and the motion consists of independent harmonic vibrations (normal modes), each with its own frequency (v). The phonon density of states $g(v)$ summed over k-space can then be used to evaluate thermodynamic properties such as the vibrational contribution to: the internal energy, U_{vib}, the Helmholtz freeenergy, A, and the entropy, S.

We considered the free energy of segregation to the $(01\bar{1}2)$ surface at 300 K for six of the ten cations (Al^{3+}, Cr^{3+}, Ho^{3+}, Lu^{3+}, Tb^{3+} and Y^{3+}). For these ions a slab of depth 17 Å with a vacuum gap 17 Å was sufficient to ensure convergence of the free-energies. The size of the simulation cell required to study the $(00-01)$ using lattice dynamics was beyond the computer resources available to us.

The number of non-equivalent configurations considered makes it possible to estimate the configurational entropic contribution to the system via the partition function. The partition function Q is defined as:

$$Q = \sum_{i=1}^{n} \exp(-(E_i - E_0)/RT) ,$$

where E_i is the energy of configuration i, E_0 is the minimum energy observed, T is the absolute temperature and R is the gas constant. Using this partition function it is possible to estimate the proportion of each configuration present as a function of temperature. In addition, by using the standard statistical thermodynamic relationship ($A_{config} = E_0 - RT \ln Q$) the configurational free energy of segregation can be evaluated as a function of temperature.

Intuitively, we would expect the relative size of the impurity ion to affect the segregation process. Indeed, many segregation models have been proposed based on this supposition (Davies et al. 1989; Davies 1992). One such model of segregation (McLean 1957) states that the primary driving force for isovalent impurity segregation is the elastic strain $U_{elastic}$, induced in the bulk lattice by the impurity. This is related to the difference in the size of the impurity and host cation, Δr by

$$U_{elastic} = 6\pi r^3 (\Delta r/r)^2/(1 + 3B/4\mu) \ ;$$

where r is the radius of the lattice cation, B is the bulk modulus of the impurity and μ is the shear modulus of the host lattice. So if it is assumed that the bulk modulus is constant for all ten impurity ions, then $U_{elastic}$ and hence the segregation energy, would be proportional to $(\Delta r \ r)^2$ The validity of this assumption has been tested by plotting the optimum segregation energy against the ratio $(\Delta r \ r)^2$ and the calculated significance of the fit for each surface considered. These results are reported later in this paper.

The structure of haematite

Hematite has the corundum structure and its space group is $R\bar{3}c$. The Fe^{3+} cations fill two-thirds of the octahedral sites created by the close-packed oxygen anion layers. It is stable under atmospheric conditions (Henderson et al. 1998) and consequently is one of the most abundant iron oxides, occurring mainly in sediments or in the soil as a product of iron-bearing minerals.

The experimentally determined unit-cell parameters, used as a starting point for this work were those reported by Howard et al. (1991) and had dimensions $a = 5.03$ Å, $b = 5.03$ Å, $c = 13.77$ Å, which on relaxation, using constant pressure energy minimization, became $a = 5.06$ Å, $b = 5.06$ Å, $c = 13.36$ Å. The structure was then cut to create the required low index surfaces and the surface energy calculated. The two most stable surfaces, the $(01\bar{1}2)$ and (0001), were then chosen for the segregation study because in addition to being the most stable, previous work (Redfern 1999) had shown them to be the most significant surfaces of haematite. This point is illustrated in Table 2, where γ, the surface energy, is reported for five of the lowest index surfaces of haematite. The order of increasing surface energies before relaxation is: $(01.2) < (11.0) < (10.1) < (00.1) < (10.0)$, but on relaxation, the order becomes: $(01.2) < (00.1) < (10.0) \approx (11.0) < (10.1)$. The (0001) and $(10\bar{1}0)$ surfaces have the largest relaxations. The surface energy of these two faces is reduced by over
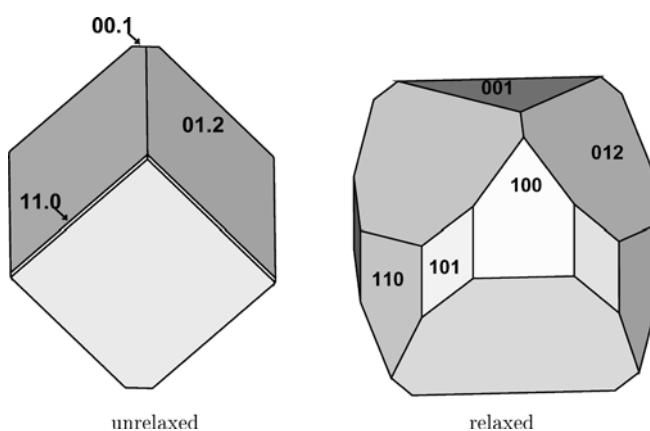
50% on relaxation, the largest changes of all terminations considered. The $(01\bar{1}2)$ face remains the most stable both before and after relaxation and undergoes the smallest relaxation of all the surfaces considered. As a way of expressing the relative surface energies we evaluated a Wulff construction (Wulff 1901), which corresponds qualitatively to the morphology of the crystal. The calculated unrelaxed and relaxed morphology of haematite, using is approach, are shown in Fig. 1.

The $(01\bar{1}2)$ surface

The lowest energy termination of the $(01\bar{1}2)$ is non-dipolar, with both Fe and O at the surface. The iron atoms have five nearest-neighbour oxygen anions, four in the surface plane and one in the plane below (Henrich and Cox 1994). These incomplete oxygen octahedra are alternately tilted with respect to the surface plane, leading to a slightly corrugated surface (Fig. 2) (Lad and Henrich 1988; Gautier et al. 1996). This surface has been calculated as being the most stable of the low index surfaces of haematite under dry conditions (Parker et al. 1999). It undergoes the least relaxation of all the haematite surfaces considered, with the surface energy reducing by only 27.8%. This is because the surface is close to bulk termination, with a decrease of just 0.05 Å (Table 3) in interplanar spacing between the two surface layers (Redfern 1999).

The (0001) surface

The (0001) surface is composed of two types of atomic plane, each consisting of either cations or anions. The cation plane is not flat and instead has half of the Fe^{3+} ions closer to the oxygen layer above and half-closer to the oxygen layer below. The creation of the cation-terminated face can be thought of as cleaving between the two sublayers of cations, thus producing a non-dipolar surface (Becker et al. 1996; Wang et al.

Table 2 Calculated surface energies of hematite

Surface	$\gamma_{unrelaxed}$ (J/m^{-2})	$\gamma_{relaxed}$ (J/m^{-2})	Change %
(0001)Fe	5.06	2.41	52.4
(0001)O	11.95	3.74	68.7
(01$\bar{1}$2)	2.91	2.10	27.8
(1000)	5.51	2.43	55.8
(1100)O	3.93	2.44	37.9
(1100)Fe	13.34	3.36	74.8
(10$\bar{1}$1)	4.86	2.97	38.9

Fig. 1 The calculated relaxed and unrelaxed morphology of hematite

Fig. 2 The structure of, **a** the (01$\bar{1}$2), **b** Fe-terminated (00.1) and **c** oxygen terminated (00.1) surfaces of hematite

(a)   (b)   (c)
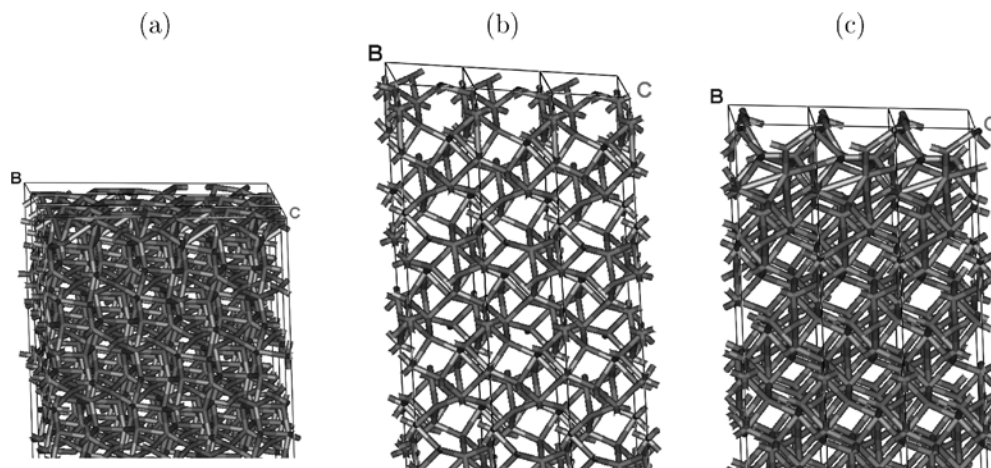
Table 3 Relaxation perpendicular to the (01$\bar{1}$2) face

Surface	Species	Height before relaxation (Å)	Height after relaxation (Å)	Change (Å)
(01$\bar{1}$2)				
	O	0.10	0.22	0.12
	Fe	0.38	0.43	0.05
	O	1.18	1.03	−0.15
	Fe	1.98	1.94	−0.04
	O	2.27	2.32	0.05
	O	3.76	3.72	−0.04
	Fe	4.05	4.06	0.01

Table 4 Relaxation perpendicular to the (0001)

Surface	Species	Height before relaxation (Å)	Height after relaxation (Å)	Change (Å)
(0001) Fe				
	Fe	0.10	0.56	−0.46
	O	0.86	0.91	−0.05
	Fe	1.63	1.70	−0.07
	Fe	2.32	2.10	0.22
	O	3.09	3.05	−0.04
(0001) O				
	O	0.86	0.84, 1.22	−0.02, 0.36
	Fe	1.63	1.21, 1.71	−0.42, 0.08
	Fe	2.32	1.86, 2.80	−0.46, 0.48
	O	3.09	2.12, −3.39	−0.97, 0.30
	Fe	3.85	3.28, 3.80	−0.57, 0.05
	Fe	4.55	4.40, 5.11	−0.15, 0.56
	O	5.31	5.05, 5.56	−0.26, 0.25

1998; Eggleston 1999). In contrast, the oxygen plane is close-packed and flat. Thus producing a non-dipolar surface involves cleaving the oxygen layer, leaving half of the O^{2-} ions at the surface.

Of the two terminations of the (0001) surface studied, the Fe-terminated surface is the dominant configuration under ultra-high vacuum conditions (Condon et al. 1995, 1998). A point reflected in its lower surface energy, 2.41 J m^{-2} as opposed to 3.74 J m^{-2} for the oxygen-terminated surface (see Table 2). The Fe-terminated surface structure is well ordered. Each cation has three oxygen neighbours in the plane below, half the number of neighbours in the bulk crystal. On relaxation, the surface energy reduces by over 50%, which is due to the iron atoms relaxing into the crystal to increase their coordination, thereby reducing the interplanar spacing between the uppermost layers from 0.85 to 0.35 Å (Table 4), a result which is well-documented for many corundum-structured oxides, for example, alumina (Kenway et al. 1989; Mackrodt at al. 1987) and chromia (Lawrence et al. 1988; Rohr et al. 1997).

The surface energy of the oxygen-terminated (0001) face is much higher and consequently it is unlikely to occur under ultra-high vacuum conditions. However, when air is introduced, especially when water vapour is present, the O-terminated surface has also been observed (Shaikhutdinov and Weiss 1999; Ketteler et al. 2001). The surface ion density of this termination is lower than

the Fe plane due to the formation of oxygen vacancies. The relaxation of this termination is very large, illustrated by the large reduction of the surface energy to 68.7% of its bulk terminated energy, as the ions relax to stabilize the surface vacancies. The relaxation of both terminations is described in terms of the change in interlayer spacing in Table 4. The effects of impurities on both surface terminations are considered in this work and their structures are shown in Fig. 2.
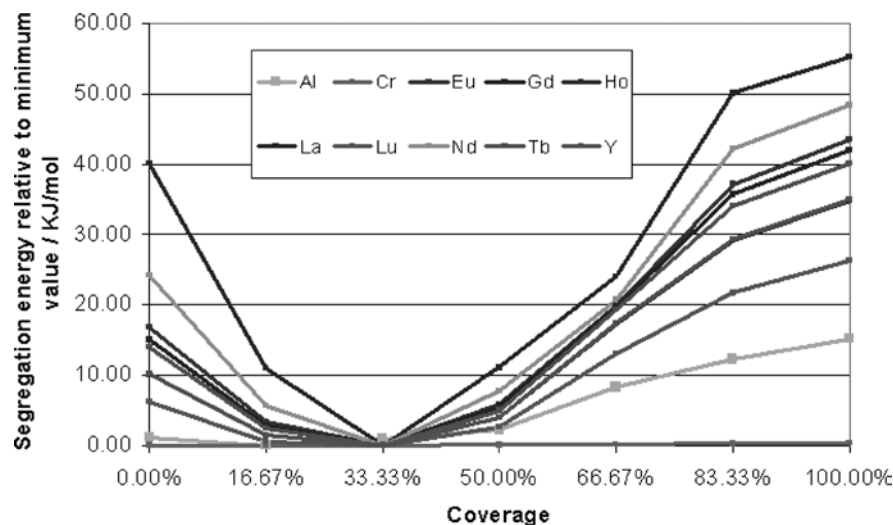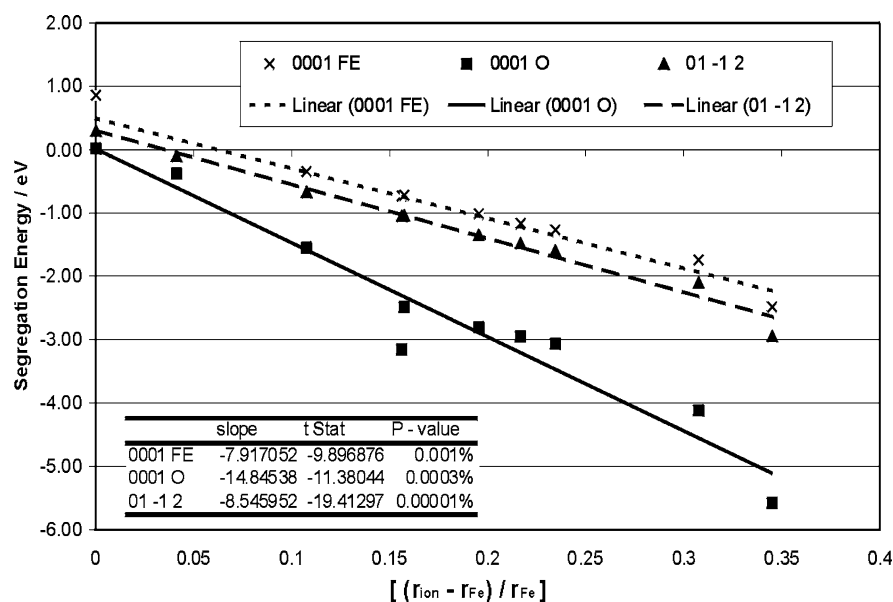
Segregation to the low-index surfaces of haematite

Segregation to the (01$\bar{1}$2) surface

The calculated energies for a cation segregating from the bulk structure to the (01$\bar{1}$2) surface as a function of coverage are given for each of the ten species in Table 5. With the exception of the two smallest ions (Al^{3+} and Cr^{3+}) the energies are negative, implying that the rare-earth cations would segregate to the (01$\bar{1}$2) surface from the bulk structure. Figure 3 shows the segregation energy plotted relative to the minimum energy observed,

Table 5 Calculated segregation energies in kJ mol^{-1} for ten cations to the dry (01 $\bar{1}$2) surface of Fe_2O_3

	Coverage (%)						
	0.00	16.67	33.33	50.00	66.67	83.33	100.00
Al^{3+}	−8.7	−9.6	−8.7	−7.7	−1.0	2.9	5.8
Cr^{3+}	28.9	28.9	28.9	28.9	28.9	28.9	28.9
Lu^{3+}	−57.9	−63.7	−64.6	−61.8	−51.1	−42.5	−38.6
Ho^{3+}	−89.7	−98.4	−99.4	−95.5	−83.0	−70.4	−64.6
Y^{3+}	−90.7	−99.4	−101.3	−97.4	−83.9	−71.4	−66.6
Tb^{3+}	−115.8	−127.4	−129.3	−124.5	−110.0	−95.5	−89.7
Gd^{3+}	−127.4	−139.9	−142.8	−137.0	−122.5	−107.1	−100.3
Eu^{3+}	−137.0	−150.5	−153.4	−147.6	−134.1	−116.7	−110.0
Nd^{3+}	−178.5	−196.8	−202.6	−194.9	−181.4	−160.2	−154.4
La^{3+}	−244.1	−273.1	−284.6	−273.1	−260.5	−234.5	−228.7

as a function of coverage, and in each case clearly shows common optimum coverage when 33.33% of the available cation sites are occupied by impurity cations.

Inspection of Fig. 3 also reveals that the magnitude of the segregation energy increases as the ionic radius of the impurity increases. For example, the optimum segregation of La^{3+}, the largest cation considered, is calculated as being −284.6 kJ mol^{-1}. In the case of smaller cations, such as Y^{3+} and Lu^{3+}, the optimum segregation energy is calculated as being −101.3 kJ mol^{-1} and −64.6 kJ mol^{-1} respectively. Indeed when the optimum segregation energy, for the ten cations, is plotted against the ratio $(\Delta r/r)^2$ in Fig. 4 a linear relationship is observed, as predicted by McLean (1957) and the equation described above. More rigorous statistical analysis reveals that the fit is highly significant, with the gradient of the line representing a true description of the data at the 0.0001% confidence level, thus illustrating that the segregation to this surface can be modelled effectively using a simple model based on relative ionic size.

Of the 15 possible configurations for replacing two of the six surface Fe^{3+} ions with dopant cations (corre-

Fig. 3 Plot of segregation energy against coverage for the (01$\bar{1}$2) surface of hematite

Fig. 4 Plot of segregation energy against relative ionic radius for the ten iso-valent impurities
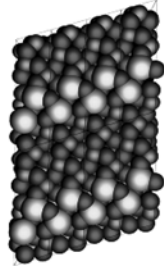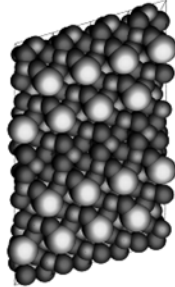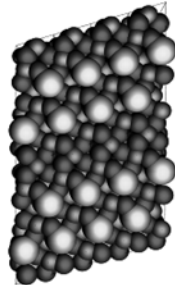
sponding to 33.3% coverage, the observed minimum in the energy curve), only three different segregation energies are calculated. The remaining 12 configurations are equivalent to one of these structures by symmetry. The distribution of the 15 configurations is, however not uniform. Instead they occur in a ratio of 6:6:3, and since the energies of non-equivalent configurations have been calculated, it is possible to evaluate a partition function for the system. Using this partition function and the relative contribution of each of the 15 structures, it is possible to predict the proportion of each structure that will be occupied by each configuration as a function of temperature.

Table 6 shows the calculated segregation energy for each of these structures and the predicted proportion of each configuration that would be observed at a macroscopic scale, over a range of temperatures. From this information it follows that at low temperatures, as expected, the lowest-energy configuration dominates in practically all cases. At higher temperatures, when the system has sufficient thermal energy, the other configurations would be occupied. It is also noted that the energy difference is small between configuration b and configuration c (typically less than 8 kJ mol^{-1}) and as there are twice as many ways of forming configuration b, at high temperatures configuration b would be predicted to dominate.

These results are, of course, based on a partition function calculated from only 15 points and are therefore approximate. They do, however, give scope for further study, by both simulation and experiment. Perhaps most importantly they serve as a reminder that a single static energy minimization is not enough to fully understand a system, and that far more information can be obtained by extending the number of points in phase space (Lavrentiev et al. 2003).

Table 6 The three non-equivalent 33.33% coverage configurations and the estimated proportion of each seen at a macro-level

		Segregation Energy / kJmol^{-1}	Temperature / K					
			1	300	600	900	1200	1500
(a)	Al^{3+}	-3	0%	8%	20%	26%	29%	31%
	Cr^{3+}	29	0%	39%	39%	40%	40%	40%
	Eu^{3+}	-126	0%	0%	0%	2%	5%	8%
	Gd^{3+}	-116	0%	0%	1%	3%	6%	9%
	Ho^{3+}	-79	0%	0%	2%	5%	9%	13%
	La^{3+}	-244	0%	0%	0%	1%	3%	5%
	Lu^{3+}	-51	0%	0%	5%	11%	15%	19%
	Nd^{3+}	-171	0%	0%	0%	2%	4%	7%
	Tb^{3+}	-104	0%	0%	1%	3%	6%	9%
	Y^{3+}	-81	0%	0%	1%	5%	9%	13%
(b)	Al^{3+}	-8	0%	57%	51%	48%	46%	45%
	Cr^{3+}	29	0%	41%	40%	40%	40%	40%
	Eu^{3+}	-149	0%	26%	45%	51%	53%	54%
	Gd^{3+}	-139	0%	29%	47%	53%	54%	54%
	Ho^{3+}	-97	0%	42%	54%	56%	55%	54%
	La^{3+}	-274	0%	4%	26%	41%	48%	51%
	Lu^{3+}	-63	0%	52%	57%	56%	54%	52%
	Nd^{3+}	-196	0%	13%	36%	45%	49%	51%
	Tb^{3+}	-126	0%	33%	49%	54%	55%	54%
	Y^{3+}	-99	0%	42%	54%	56%	55%	54%
(c)	Al^{3+}	9	100%	35%	29%	27%	25%	24%
	Cr^{3+}	29	94%	20%	20%	20%	20%	20%
	Eu^{3+}	-154	100%	74%	54%	46%	41%	38%
	Gd^{3+}	-143	100%	71%	52%	45%	40%	37%
	Ho^{3+}	-100	100%	58%	45%	39%	36%	33%
	La^{3+}	-266	100%	96%	74%	58%	50%	44%
	Lu^{3+}	-65	100%	48%	38%	34%	31%	29%
	Nd^{3+}	-202	100%	87%	64%	53%	47%	42%
	Tb^{3+}	-130	100%	67%	50%	43%	39%	36%
	Y^{3+}	-101	100%	58%	45%	39%	36%	33%

Fig. 5 Plot of free energy of segregation energy against coverage for the (01 12) surface of hematite
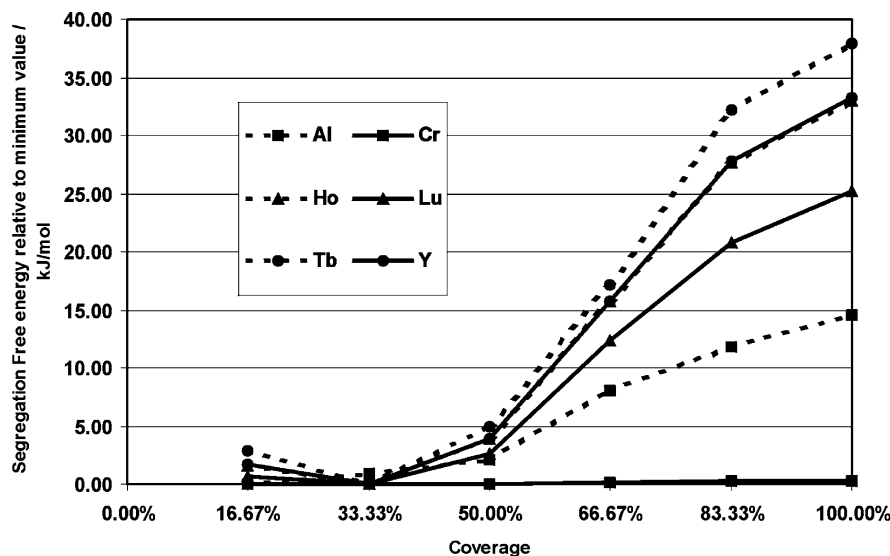

As stated above, it is possible to go beyond calculation of the static lattice energy of a system and calculate the vibrational contribution to the free energy using lattice dynamics. Additionally, we are able to estimate the effect of the vibrational component on the configurational free energy by calculating the partition function from the 64 configurations considered. The results for seven of the cations at 300 K are presented graphically in Fig. 5; again the calculated energies are plotted relative to the minimum calculated energy. On inspection it is clear that the same general trends are followed as in the static case. An energy minimum is calculated at 33.33% coverage with the exception of Cr^{3+}, which once again is predicted to exhibit Langmuir behaviour. The vibrational effects are small (typically less than

10 kJ mol^{-1}) with the majority of this difference resulting from the zero-point contribution to the vibrational free energy, rather than the vibrational entropy contribution. Further calculations reveal that this is still the case at higher temperatures.

The small effect of the vibrational contribution to the surface free-energy is further illustrated by considering the phonon density of states diagrams for pure and doped surfaces. An example of such a comparison is shown in Fig. 6. The $g(v)$ for the pure (01$\bar{1}$2) surface of haematite is compared with the $g(v)$ for 100% surface coverage of Al^{3+}, Y^{3+} and Tb^{3+}. In all three cases the differences in the distributions are evident across the entire frequency range. This indicates that the differences are due to small frequency shifts, rather than significant additional modes in specific parts of the frequency spectrum. Further evidence for this also comes from the fact that all differences between the

Fig. 6 Calculated difference in density of states diagrams at 300 K and 100% coverage *Top* Al^{3+}; *middle* Y^{3+}; *bottom* Tb^{3+}
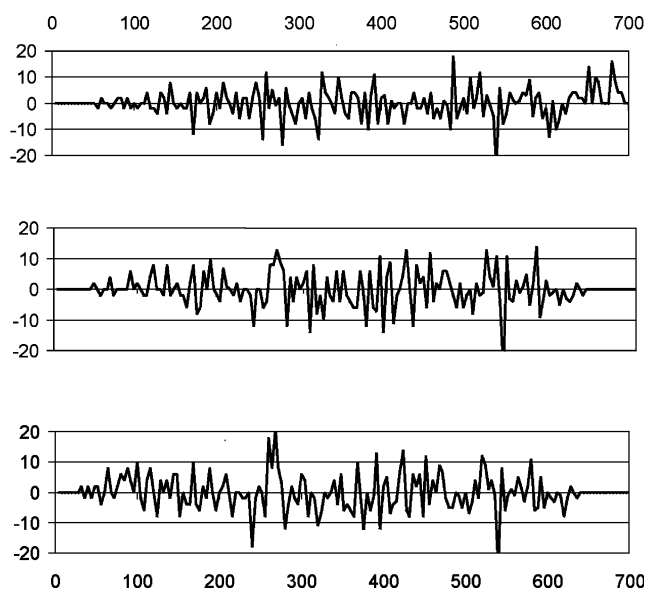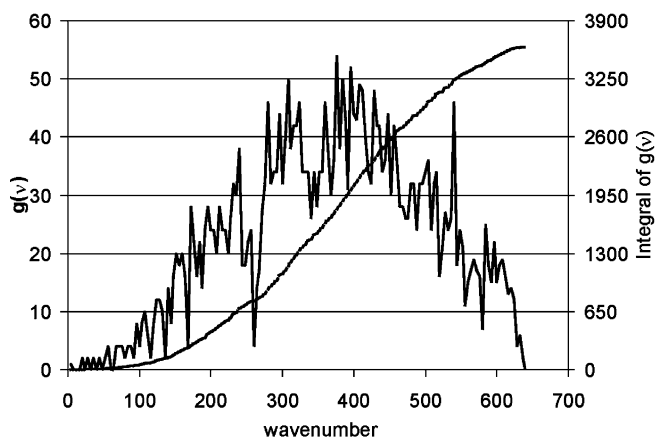
**Table 7** Calculated segregation energies in kJ mol^{-1} for ten cations to the dry (0001) Fe-terminated surface of Fe$_2$O$_3$

	Coverage %						
	0.00	16.67	33.33	50.00	66.67	83.33	100.00
Al^{3+}	−35.7	−36.7	−35.7	−35.7	−34.7	−33.8	−33.8
Cr^{3+}	83.0	83.0	83.0	83.0	83.0	83.0	83.0
Lu^{3+}	−33.8	−33.8	−32.8	−32.8	−29.9	−28.0	−26.1
Ho^{3+}	−70.4	−69.5	−68.5	−66.6	−65.6	−61.8	−58.9
Y^{3+}	−69.5	−68.5	−67.5	−63.7	−65.6	−59.8	−56.9
Tb^{3+}	−97.4	−96.5	−95.5	−93.6	−85.9	−91.7	−81.0
Gd^{3+}	−112.9	−111.0	−110.0	−106.1	−107.1	−98.4	−94.6
Eu^{3+}	−122.5	−120.6	−119.6	−116.7	−115.8	−110.0	−102.3
Nd^{3+}	−167.9	−165.0	−165.0	−161.1	−159.2	−150.5	−140.9
La^{3+}	−240.2	−233.5	−234.5	−227.7	−225.8	−211.3	−200.7

Table 8 Calculated segregation energies in kJ mol^{-1} for ten cations to the dry (00.1) O-terminated surface of Fe$_2$O$_3$

	Coverage (%)						
	0.00	16.67	33.33	50.00	66.67	83.33	100.00
Al^{3+}	−35.7	−36.7	−31.8	−26.1	−22.2	−18.3	−13.5
Cr^{3+}	1.9	15.4	1.9	21.2	28.0	32.8	37.6
Lu^{3+}	−3.9	−92.6	−149.6	−111.0	−82.0	−54.0	−44.4
Ho^{3+}	−19.3	−240.2	−164.0	−148.6	−111.9	−108.1	−74.3
Y^{3+}	−20.3	−276.9	−303.9	−230.6	−138.0	−149.6	−117.7
Tb^{3+}	−35.7	−271.1	−226.7	−185.3	−152.4	−134.1	−99.4
Gd^{3+}	−43.4	−284.6	−221.9	−198.8	−165.0	−146.7	−112.9
Eu^{3+}	−50.2	−295.2	−251.8	−210.3	−173.7	−155.3	−137.0
Nd^{3+}	−83.0	−397.5	−303.0	−257.6	−218.1	−231.6	−178.5
La^{3+}	155.3	−447.7	−538.4	−428.4	−435.1	−389.8	−247.0

distributions are low in intensity (< 20 out of total distribution of 4000 modes) and that the differences are centred around zero. In summary, we find that the vibrational contribution to the segregation free energy is small and can therefore be neglected with minimal loss of accuracy.
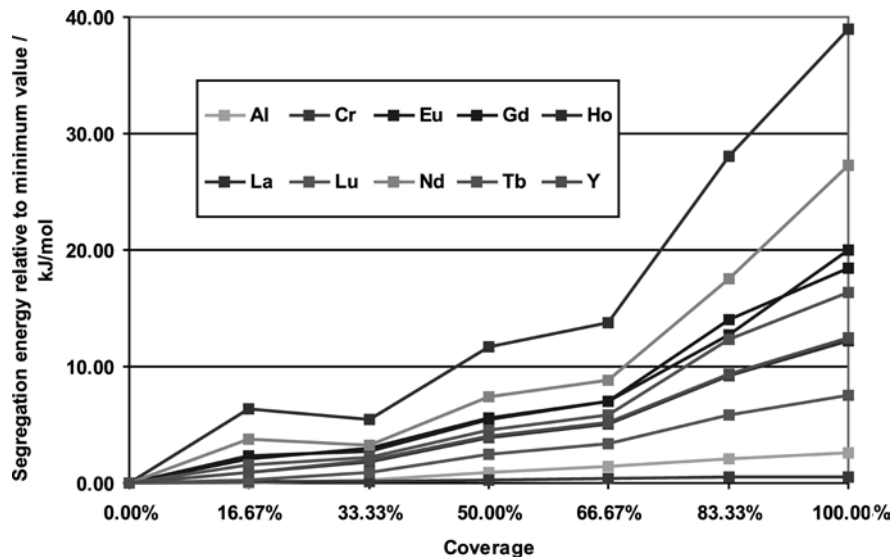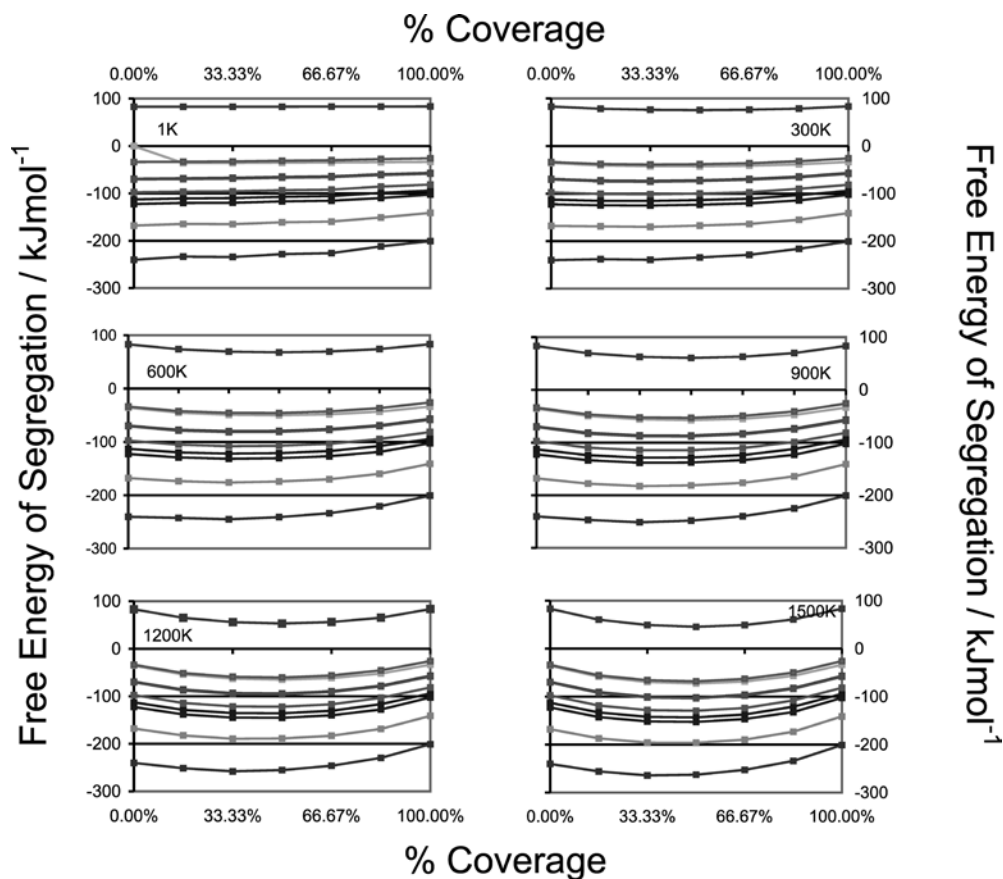
Segregation to the (0001) surface

The segregation energy has also been calculated for the ten impurities segregating to each of two (0001) terminations, i.e. the Fe and O terminations. The results are displayed in Tables 7 and 8 below.

The minimum in the energy/coverage plots is observed at zero coverage for the Fe-terminated (0001) surface (Fig. 7). The results suggest that segregation to the (0001) Fe-terminated surface occurs only when there is a high concentration of dopant cations in the bulk structure. These results also explain why this surface can be generated in ultra-high vacuum conditions since, once clean, there is very little driving force for segregation. For nine of the ten cations the segregation energy is calculated as being negative. The exception is Cr^{3+}. Interestingly the results for Cr^{3+} are independent of coverage and the segregation energy is calculated to be 83 kJ mol^{-1} (0.86 eV). Once again, it is noted that the optimum segregation energies increase with increasing ionic radius of the impurity. For example La^{3+} $r = 1.016$ Å, $E_{seg} = -240.2$ kJ mol^{-1}; Y^{3+} $r = 0.893$ Å, $E_{seg} = -70.4$ kJ mol^{-1} and Lu^{3+} $r = 0.85$ Å, $E_{seg} = -33.8$ kJ mol^{-1}. In addition, when the optimum segregation energy is plotted against the ratio $((\Delta r/r)^2$ (Fig. 4) a linear relationship in accordance with the segregation model proposed above is calculated. Statistical analysis reveals that the fit is highly significant, with the gradient of the line representing a true description of the data at the 0.001% confidence level, again illustrating the validity of using a model based on relative ionic size.

The configurational free energy of segregation ($A_{config} = E_0 - RT \ln Q$) as a function of temperature was estimated. Again, we assume that the 64 configurations considered adequately represent all of phase space. This approximation means that the results obtained from such a procedure are only qualitative, but even so can reveal an underlying trend that static calculations alone cannot predict.

Fig. 7 Plot of segregation energy against coverage for the iron terminated (0001) surface of heamatite

Fig. 8 Plot of configurational segregation energy against % coverage over a temperature range varying from 1 to 1500 K

Fig. 9 Plot of segregation energy against coverage for the oxygen terminated (0001) surface of hematite
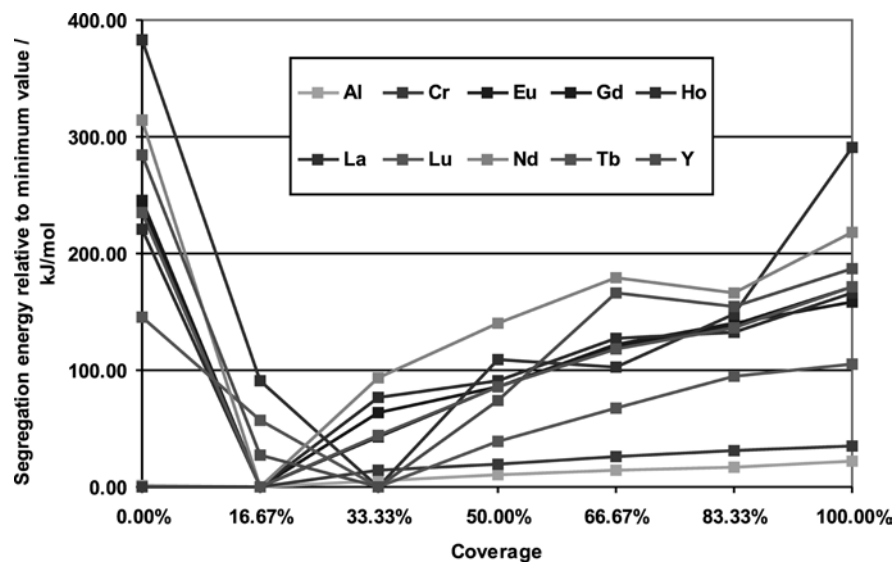
These results are plotted in Fig. 8 at 300 K intervals over the range 0 to 1500 K. The variation of free energy with composition is much smoother at high temperatures, compared to those generated at low temperatures and when only lattice energy is considered. At high temperatures, there is now a calculated minimum in free energy at approximately 33.3% coverage of impurity. Thus, considering the high temperatures, we again predict that a surface with a 33% impurity composition is

preferred, something not predicted when considering the lattice energy alone.

Finally, we considered the oxygen-terminated (0001) surface. There is again a minimum in the segregation energy/coverage plot at a non-zero coverage (Fig. 9). However, unlike the (01$\bar{1}$2) surface, where the minimum always occurred at the same coverage for all the ions studied, the minimum energy was found at 16.67% for Al^{3+}, Cr^{3+}, Eu^{3+}, Gd^{3+},

Ho^{3+}, Nd^{3+} and Tb^{3+}; and at 33.33% for La^{3+}, Lu^{3+} and Y^{3+}.

There are several possible explanations for the different minimum compositions for the oxygen-terminated (0001) surface. First, it could be related to the size of the segregating ion. For example, steric hindrance might result in there being too little space for those ions where the energy minimum is at 16.67% coverage to adopt configurations at higher concentrations. This is an unlikely explanation because examination of the impurity ions and their calculated optimum coverage reveals no correlation between ionic radius and the position of the energy minimum. For example, the largest ion, La^{3+} is calculated to have an optimum coverage of 33.3%, whereas the energy minimum for the smallest ions, Al^{3+} and Cr^{3+}, appears at the lower coverage. Further evidence for rejecting this explanation comes from the fact the Ho^{3+} and Y^{3+} have remarkably similar ionic radii (both 0.89 Å) but the optimum coverage is calculated at different concentrations of impurity.

A second possible explanation is that since only seven points are considered, there are an insufficient number of points to precisely locate the true energy minimum, which may lie at a point somewhere between 16.67 and 33.33% coverage. Preliminary calculations using a smaller unit cell with four surface cations did reveal a minimum at 25% coverage; however, in many cases this point was of higher energy than the calculated minima in the original calculations with six surface cations. Work with larger unit cells, in order to search a larger portion of configuration space, will therefore be required to confirm or refute this hypothesis.

A third explanation is that the difference in minima illustrates the existence of a more complex surface or inter-ionic phenomena, which has so far been overlooked. This is, however, counteracted by the fact that once again an excellent fit is predicted when the segregation energy is plotted against the ratio $(\Delta r/r)^2$ (Fig. 4). Statistical analysis reveals that the fit is highly significant, with the gradient of the line representing a true description of the data at the 0.0001% confidence level, confirming a model based on ionic radius that adequately describes the segregation to this surface.

Conclusion

The work presented in this paper illustrates how the heavy-metal impurities affect the stability of two of the important low index surfaces of haematite. In common with previous experimental and theoretical studies, we found the (0001) and (01$\bar{1}$2) surfaces to be the most stable low index surfaces and consequently predict that they would dominate the morphology of the crystal. Thus it was these two surfaces that were considered in the segregation study.

Our work has found that the segregation of the dopant ions from the bulk structure to the surfaces of interest is in practically all cases exothermic and thus energetically favoured. In the case of the (01$\bar{1}$2) surface the minimum energy is greatest when the surface concentration of impurity is 33.33%. There is no obvious phase that the surface is attempting to adopt with this composition. Although it is tempting to believe that it is attempting to form a disordered garnet (where the optimum impurity composition would be 37.5%). In addition, the optimum concentration is independent of cation size, while the depth of the minimum at the optimum concentration increases as the size of the dopant cation increases. For example the optimum segregation energy was calculated as being $-64.6\sim$ kJ mol^{-1} for Lu^{3+} ($r = 0.85$ Å) and -284.6 kJ mol^{-1} for La^{3+} (r = 1.016 Å). Indeed more formal statistical analysis revealed that there was a highly significant correlation between the segregation energy and the square of the relative size of the impurity.

At the optimum coverage 15 possible configurations of the impurity on the surface were considered. It was found that all of these represented one of three degenerate structures. By considering the relative contribution of each to the free energy, we predict that as the temperature is raised, the preferred geometry of the system will change. At higher temperatures the less favoured structures become occupied and because of symmetry effects we predict that on the macroscopic scale the optimum surface phase will appear more disordered and composed of domains of the lower-energy configurations.

When the Fe termination of the (0001) surface was considered, the optimum segregation energy was predicted as occurring at zero coverage of impurity, suggesting that segregation would occur only when there is a high concentration of impurity in the bulk structure. However, we predict that the 33.33% coverage of impurity becomes energetically favoured as the temperature is increased towards 1500 K. The results are different from those of the oxygen-terminated surface where the minimum energy configuration varies between 16.67 and 33.33% depending on the cation. and Whilst the magnitude of the optimum coverage once more varies with the square of the relative size of the impurity, there is no obvious correlation between the size of the dopant cation the optimum coverage. This suggests that the true energy minimum lies at coverage between these two values, something future work with larger simulation cells could determine.

In summary, the simulations predict that the rare-earth cations will segregate to the low index surfaces of haematite. The results suggest that the surface may begin to form a surface phase with a composition not unlike the iron–rare-earth garnets. However, at the macroscopic level we would expect the surface structure to be disordered.

Subsequent work will extend the discussion to consider hydoxylated and hydrated surfaces, thus simulating more closely the conditions found in the environment.

References

Arocena JM, Pawluk S, Dudas MJ (1992) genesis of selected sandy soils in Alberta, Canada, as revealed by microfabric, leachate composition and soil composition. Geoderma 54: 1–4

Barron THK, Collins CM, White GK (1980) Adv Phys 20: 609

Beenasik AB, Janowski J, Hirschwald W, Noworthy J, Janowski ABJ, Stolze WHF, Nowotny (1991) Effect of surface treatment on segregation of impurities in haematite. J Mater Sci 26: 2527–2532

Becker U, Hochella MF, Apra E (1996) The electronic structure of haematite {001} surfaces: applications to the interpretation of STM images and heterogeneous surface reactions. Am Mineral 81(11–12): 1301–1314

Born M, Huang K (1954) Dynamical theory of crystal lattices. Oxford University Press, Oxford, UK

Bryan ND, Heketh N, Livens FR, Tipping E, Jones MN (1998) Metal ion–humic substances interaction, a thermodynamic study. J Chem Soc Faraday T 94(1): 95–100

Cochran JW (1973) The dynamics of atoms in crystals. Edward Arnold, London, UK

Condon NG, Leibsle FM, Lennie AR, Murray PW, Vaughan DJ, Thornton G (1995) Biphase ordering of iron–oxide Surfaces. Phys Rev Lett 75(10): 1961–1964

Condon NG, Leibsle FM, Lennie AR, Murray PW, Parker TM, Vaughan DJ, Thornton G (1998) Scanning tunnelling microscopy studies of α-Fe$_2$O$_3$(0001). Surf Sci 397(1–3): 278–287

Cotter M Campbell S, Cao LL, Egdell RG, Mackrodt WC (1989) Surface segregation of Ba in MgO. Surf Sci 208(3): 267–284

Davies MJ, (1992) Computer simulation of oxide surfaces and grain boundaries. PhD Thesis University of Bath, Bath, UK

Davies MJ, Kenway PR, Lawrence PJ, Parker SC, Mackrodt WC, Tasker PW (1989) Impurity segregation to the surfaces of corundum-structured oxides. J Chem Soc Faraday T II 85: 555–563

Dick BG, Overhauser AW (1958) Theory of dielectric constants of alkali halide crystals. Phys Rev 112(1): 90–103

Duffy DM, Tasker PW, (1983) A guide to CHAOS: a program for the calculation of point defect energies near interfaces in ionic crstals. Harwell Technical Report, AERE, Harwell, Oxon, UK R11059

Eggleston CM (1999) The surface structure of α-Fe$_2$O$_3$ (001) by scanning tunneling microscopy: implications for interfacial electron transfer reactions. Am Mineral 84 (7–8): 1061–1070

Ewald PP (1921) Die Berechnung optisher und elektrostatisher Gitterpotentiale. Ann Phys 64: 253–287

Gautier Soyer M, Pollak M, Henriot M, Guittet MJ (1996) The (1 × 2) reconstruction of the α-Fe$_2$O$_3$ ($\bar{1}$012) surface. Surf Sci 352: 112–116

Harding JH, Atkinson, KJ, Grimes RW, (2003) Experiment and theory of diffusion in alumina. J Am Ceram Soc 86(4): 554–559

Henderson MA, Joyce SA, Rustad JR (1998) Interaction of water with the (1 × 1) and (2 × 1) surfaces of α-Fe$_2$O$_3$. (012) Surf Sci 417(1): 66–81

Henrich VE, Cox PA (1993) Fundamentals of gas–surface interactions on metal-oxides. Appl Surf Sci 72(4): 277–284

Howard CJ, Sabine TM, Dickson F (1991) Structural and thermal parameters for rutile and anatase. Acta Crystallogr 47: 462–468

Kenway PR, Parker SC, Mackrodt WC (1989) Alkaline-earth impurity segregation to the basal and prism surfaces of alumina. Mol Simulat 4: 175–185

Ketteler G, Weiss W, Ranke W, Schlogl R (2001) Bulk and surface phases of iron oxides in an oxygen and water atmosphere at low pressure. Phys Chem Chem Phys, 3(6): 1114–1122

Lad RJ, Henrich VE (1988) Structure of α-Fe$_2$O$_3$ single-crystal surfaces following Ar$^+$ Ion bombardment and annealing in O^{-2}. Surf Sci 193(1–2): 81–93

Lawrence PJ, Parker SC, Tasker PW (1988) Computer-simulation studies of perfect and defective surfaces in Cr$_2$O$_3$. J Am Ceram Soc 71(8): C389–C391

Lavrentiev MYu, Allan NL, Purton JA (2003) Beyond the point defect limit: solid solutions, phase diagrams and trace-element partitioning. Phys Chem Chem Phys 5(11): 2190–2196

Leslie M (1982) AERE report R11059. SERC Daresbury, Warrington, UK

Lewis GV, Catlow CRA (1985), Potential models for ionic oxides J Phys C Solid State 18(6): 1149–1161

Mackrodt WC, Davey RJ, Black SN, Docherty R (1987). The morphology of α-Al$_2$O$_3$ and α -Fe$_2$O$_3$ the importance of surface relaxation. J Cryst Growth 80 (2): 441–446

McLean D, (1957) Grain boundaries in metals. Clarendon Press, London, UK

Mott NF, Littleton MJ (1938) Conduction in polar crystals. I. electrolytic conduction in solid salts. T Faraday Soc 38: 485–499

Parker SC, de-Leeuw NH, Redfern SE (1999) Atomistic simulation of oxide surfaces and their reactivity with water. Faraday Discuss 114: 381–393

Parker SC, Price GD (1989) Computer modelling of phase transitions in minerals. Adv Solid State Chem 1: 295–327

Parker SC, de-Leeuw NH, Bourova E, Cooke DJ (2001) Application of lattice dynamics and molecular dynamics. In: Cygan JD, Kubicki RT (eds) Molecular modeling theory: applications techniques to minerals and their surfaces in the geosciences. MSA, New York, USA 42: 63–82

Parry DE (1975) Electrostatic potential in the surface region of an ionic crystal. Surf Sci 49: 433

Parry DE (1976) ERRATA —electrostatic potential in the surface region of an ionic crystal. Surf Sci 54: 195

Redfern SE (1999) Atomistic simulation of mineral surfaces their structure, hydration and growth. PhD Thesis University of Bath, Bath UK

Rohr F, Baumer M, Freund HJ, Mejias JA, Staemmler V, Muller S, Hammer L, Heinz K (1997). Strong relaxations at the Cr2O3(0001) surface as determined via low-energy electron diffraction and molecular dynamics simulations. Surf Sci 372 (1–3): L291–L297

Shaikhutdinov SK, Weiss W (1999), Oxygen pressure dependence of the α-Fe2O3(0001) surface structure. Surf Sci 432(3): L627–L634}

Suzuki T, Hishita S, Oyoshi K, Souda R (1998) Surface segregation of implanted ions: Bi, Eu, and Ti at the MgO(100) surface. Appl Surf Sci 130–132: 534–538

Tasker PW (1979) The stability of ionic crystal surfaces. J Phys (C) 12: 4977–4984

Watson GW, Kelsey ET, de-Leeuw NH, Harris DJ, Parker SC (1996) Atomistic simulation of dislocations, surfaces and interfaces in MgO. J Chem Soc Faraday T 92(3): 433–438

Watson GW, Tschaufeser P, Wall A, Jackson RA, Parker SC (1994) Lattice energy and free-energy minimisation techniques. In: Catlow CRA(ed) Computer modelling in inorganic crystallography. Academic Press, London, UK pp 55–81

Wang XG, Weiss W, Shaikhutdinov SK, Ritter M, Petersen M, Wagner F, Schlogl R, Scheffler M (1998) The haematite (α-Fe$_2$O$_3$ (0001)) surface: evidence for domains of distinct chemistry. Phys Rev Lett 81(5): 1038–1041

Wenming Dong, Xiangke Wang, Xiaoyan Bian, Aixia, Wang Jingzho, Du, Tao Zuyi (2001). Comparative study on sorption/desorption of radioeuropium on alumina, bentonite and red earth: effects of pH, ionic strength, fulvic acid, and iron oxides in red earth. Appl Radiat Isotopes 54(4): 603–610

Wulff G (1901) Zur Frage der Heschwindigkeit des Wachstums un der Auflosung der Krystalflachen. Z Kristal log 34: 449–530

Xiangke Wang, Wenming Dong, Xiongxin Dai, Aixia Wang, Jinzhou Du, Zuyi Tao (2000) Sorption and desorption of Eu and Yb on alumina: mechanisms and effect of fulvic acid. Appl Radiat Isotopes 52(2): 165–173